

Veselago lens and Klein collimator in disordered graphene

F Libisch¹, T Hisch, R Glattauer, L A Chizhova and J Burgdörfer

Institute for Theoretical Physics, Vienna University of Technology, Wiedner Hauptstraße 8-10/136, A-1040 Vienna, EU, Austria

E-mail: florian@concord.itp.tuwien.ac.at

Received 2 September 2016, revised 20 December 2016

Accepted for publication 3 January 2017

Published 7 February 2017



Abstract

We simulate electron transport through graphene nanoribbons of realistic size containing a p–n junction patterned by electrostatic gates. For a sharp p–n interface, Klein tunneling leads to refocusing of a divergent beam forming a Veselago lens. Wider transition regions allow only electrons with near-perpendicular incidence to pass the junction, forming a Klein collimator. Using a third nearest neighbor tight binding description we explore the influence of interface roughness and bulk disorder on guiding properties. We provide bounds on disorder amplitudes and p–n junction properties to be satisfied in order to experimentally observe the focusing effect and compare our predictions to very recent realizations.

Keywords: graphene, nanoelectronics, Klein tunneling, Veselago lens

(Some figures may appear in colour only in the online journal)

1. Introduction

Graphene nanostructures [1–4] continue to attract considerable attention mainly due to their potential applications in high mobility electronics [5] and solid state quantum information processing [6, 7]. Intensive research has been triggered by the unique electronic properties of graphene [8, 9] including the gapless linear dispersion, and the relativistic Landau level (LL) spectrum [10, 11]. Graphene nanostructures also promise to allow exploration of phenomena related to massless Dirac fermions in reduced dimensions [12–14] in the presence of confinement. In particular, relativistic Klein tunneling [15] can give rise to unconventional transmission properties of p–n junctions in graphene [16–18] such as the Veselago lens effect [19, 20]. Accordingly, an ideally sharp interface separating an electron

and a hole cone acts for fermions as a material with negative index of refraction similar to recently discovered metamaterials for electromagnetic radiation [21–23], resulting in effects such as ‘cloaking’ [24]. Electrostatically patterned nanoribbons can thus be viewed as the starting point for graphene-based two-dimensional electron optics with unconventional properties. Recent advances in fabricating high-quality graphene-hexagonal boron nitride (hBN) sandwich structures [25, 26] have overcome intrinsic difficulties in creating tunneling barriers and confining electrons in graphene, opening up the pathway towards graphene-based electron optics. Electrostatic gates on top of the hBN layer can now be placed much closer to the graphene sheet enabling sharper p–n junctions. While experimental realization of such electron ‘beam’ shaping and focusing devices has remained a challenge, first experimental observations have become available [27]. In this work we present theoretical simulations for electron transmission through a realistic p–n nano-scale graphene junction, and investigate its potential for electron-optical applications. Our focus is on the destructive influence of disorder on the focusing and collimation effects. We consider both a corrugated interface of the p–n junction and bulk disorder on the n- and p-side. Previous investigations of Klein tunneling in disordered p–n junctions [29–31] show that disorder improves transmission of the p–n junction. We show quantitatively that both Veselago lens effects and beam

¹ This article belongs to the [special issue: Emerging Leaders](#), which features invited work from the best early-career researchers working within the scope of *Journal of Physics: Condensed Matter*. This project is part of the *Journal of Physics* series’ 50th anniversary celebrations in 2017. Florian Libisch was selected by the Editorial Board of *Journal of Physics: Condensed Matter* as an Emerging Leader.



Original content from this work may be used under the terms of the [Creative Commons Attribution 3.0 licence](#). Any further distribution of this work must maintain attribution to the author(s) and the title of the work, journal citation and DOI.

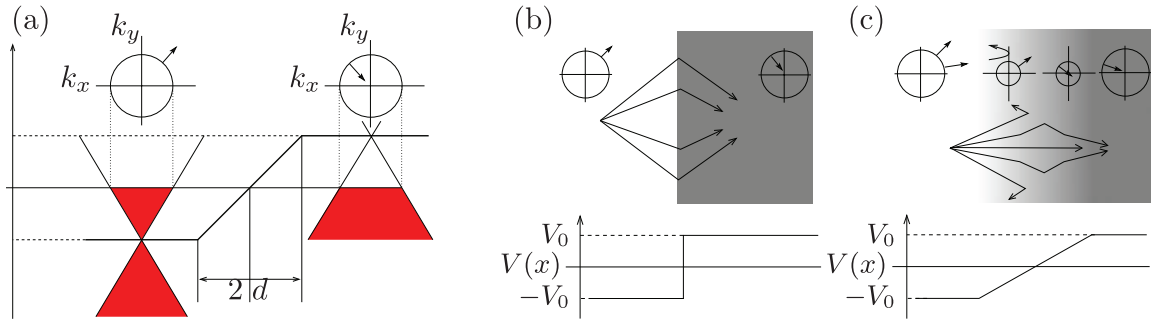


Figure 1. (a) Graphene bandstructure near a p–n junction with transition width $2d$. Circles represent cuts through the Dirac cone at constant energy, the arrow gives the direction of group velocity. (b) Refraction at an ideal infinitely sharp p–n junction with zero transition width $d = 0$ results in focusing due to the different sign of the group velocity for the particle and hole. (c) Same as (b) for a finite transition width between n- and p-region, leading to specular reflection of rays incident with large perpendicular momentum component k_y as transmission through the intermediate region is blocked (see text).

collimators are robust in the presence of moderate interface roughness and weak bulk disorder, and give quantitative constraints for experimental realizations.

2. Klein tunneling

The linear band crossing in graphene at the K -point, the so-called Dirac point creates a double-cone structure that closely mimics the dispersion relation of massless Dirac fermions (see figure 1(a)), described by the Dirac-like Hamiltonian,

$$H = v_F \begin{pmatrix} 0 & p_x + ip_y \\ p_x - ip_y & 0 \end{pmatrix} + \mathbb{1} \cdot V(\mathbf{x}), \quad (1)$$

where p_x (p_y) denote the momentum operators and we have set $E(k_K) = 0$. The approximation (1) ignores both the length scale of the graphene lattice constant $a = 1.4 \text{ \AA}$ and the broken rotational symmetry of the cone due to the hexagonal lattice structure, an effect known as trigonal warping [8]. The symmetric electron-like (hole-like) dispersion relation of equation (1) above (below) the Dirac point allows to locally tune the Fermi energy to create n-doped (electron-like) or p-doped (hole-like) regions of carrier density by an external potential. At a finite-width potential step $V(x)$ (by, e.g. a back gate) [8] (see figure 1)

$$V(x) = \begin{cases} V_0 \cdot x/d & |x| < d \\ \text{sgn}(x) \cdot V_0 & |x| \geq d \end{cases} \quad (2)$$

between an n-doped and a p-doped region, electrons may tunnel from the n-region into the p-region (see figure 1(a)). In the limit of a sharp interface with the transition half-width d small compared to the de Broglie wavelength λ_D , $d \ll \lambda_D$, tunneling occurs with near unit probability due to the electron-hole symmetry of H (equation (1)), a phenomenon known as Klein tunneling [15, 32]. Since the group velocity is reversed when switching from the upper to the lower cone, i.e. from the n to the p region, the wave originally propagating in the (k_x, k_y) direction in the n-region is transmitted into the p region with wavevector $(-1) \cdot (-k_x, k_y) = (k_x, -k_y)$ due to flux conservation at the interface. The resulting scattering kinematics corresponds to the optical analogue of a metamaterial with a negative index of refraction (figure 1). Consequently, a diverging ray of trajectories emanating from a source point

(S) will be focused by an ideal p–n interface onto the point F on the p side. Such an electron-optical lens could be created in graphene simply by applying a discontinuous potential step. If, however, the transition from n- to p- region is gradual instead of sudden, i.e. if d is of the order of λ_D , new effects appear. For grazing incidence with $|k_y| \gg |k_x|$ at the p–n interface, $|k_y|$ may exceed the local $k(x) = |E_F - V(x)|/\hbar v_F$ causing total reflection rather than transmission. Consequently, partial transmission through the p–n interface is restricted to near-normal incidence [28] and no distinct focal point exists. The p–n junction operates in this regime as filter that only transmits on near-normal incidence.

3. p–n junction in graphene nanoribbons

Realizing electron-optical elements such as lenses and filters suggested by the ideal massless Dirac fermion picture (equation (1)) in graphene structures must account for the discrete honeycomb lattice structure with lattice constant a made up by two interleaved triangular sublattices (A and B). It can be described in tight-binding approximation by the Hamiltonian [33]

$$H = \sum_i |\phi_i\rangle V_i \langle \phi_i| - \sum_{(i,j)} \gamma_{i,j} |\phi_i\rangle \langle \phi_j| + \text{h.c.}, \quad (3)$$

where the sum (i,j) extends over pairs of lattice sites, $|\phi_{i,s}\rangle$ is the tight-binding orbital with spin s at lattice site j , V_i is a locally varying potential which includes in the present case the potential step (equation (2)), and $\gamma_{i,j}$ are the hopping matrix elements between lattice sites i and j . We omit physical spin in the following. In contrast to the Dirac Hamiltonian of equation (1), the electronic structure of graphene features a weakly broken electron-hole symmetry accounted for in the present simulations by including third-nearest-neighbor coupling (for details see [34]). Furthermore, the hexagonal symmetry of the graphene lattice distorts the perfectly circular Dirac cone at energies farther away from the Dirac point. This so-called trigonal warping [8, 37] is also included in our third-nearest neighbor description.

We explore the consequences of this symmetry breaking for a graphene nanoribbon that extends to infinity to the left and right, $(x \rightarrow \pm\infty)$, containing a single p–n transition.

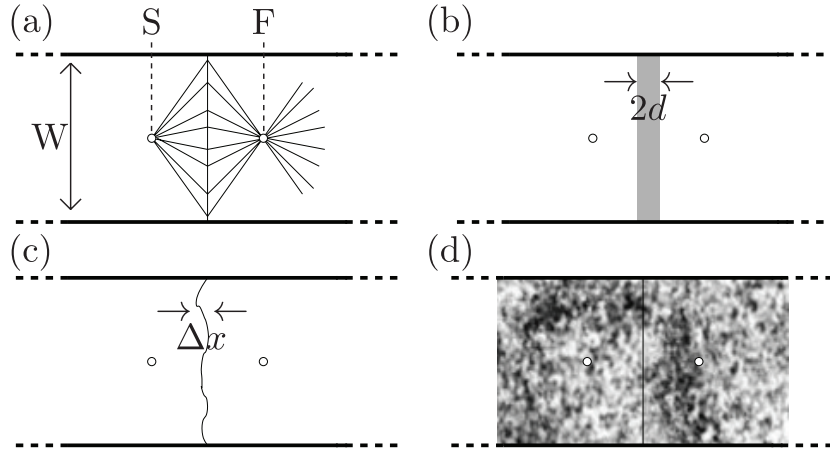


Figure 2. (a) Schematic view of the p–n junction forming a Veselago lens. Source (S) and focal point (F) are marked by open circles. Rays correspond to a perfect negative refractive index $n = -1$. We investigate the consequences of a finite transition width $2d$ (b), finite interface roughness Δx (c) and bulk disorder in the n- and p-regions (d).

Note that a flake of finite size would be unsuitable to realize focusing of rays as bound state effects of the finite-size flake would overshadow the propagation. We therefore use open boundary conditions within the framework of an effective Hamiltonian

$$H_{\text{eff}} = H + \Sigma_L(E) + \Sigma_R(E), \quad (4)$$

where the energy-dependent self-energy matrices $\Sigma_L(E)$, $\Sigma_R(E)$ describe the coupling to half-infinite waveguides to the left (L) and right (R) via $\Sigma_L = H_L G_L H_L^\dagger$, $\Sigma_R = H_R^\dagger G_R H_R$. Here, G_L and G_R represent the surface Green's functions of the perfect half-infinite waveguides, and H_I the interaction Hamiltonian between the leads and the simulated structure. H_I , and consequently the self-energy corrections Σ_L , Σ_R are non-zero only on to the outermost carbon atoms to the left and right. Note that H_{eff} is no longer Hermitian since the open boundary conditions introduce a finite lifetime of states.

The width W of the nanoribbon plays a key role for observing lens or collimator effects. Only for sufficiently large width $W \gg \lambda_D$ (for more quantitative estimates see below) pronounced lens effects appear while for smaller W distortions by reflection at the boundary largely mask the effects. The simulation of such wide ribbons (in the following we consider W between 120 and 300 nm) represents a numerical challenge. The simulation of such wide ribbons (1200 lattice sites in transverse direction for $W = 120$ nm) includes several million carbon orbitals. We consider a point source (S) on the n side (figure 2) and calculate the propagated wavefunction at the position \mathbf{x} in the ribbon, $\psi_{\mathbf{x}_S}(\bar{x})$, via the Green function G as

$$\psi_{\mathbf{x}_S}(\mathbf{x}) := G(\mathbf{x}, \mathbf{x}_S) = \langle \mathbf{x} | \frac{1}{H_{\text{eff}} - E} | \mathbf{x}_S \rangle, \quad (5)$$

where x_S is the source point of current injection. We use a parallelized, distributed matrix inversion [35, 36] suitable for the efficient description of large-scale graphene nanodevices.

We first probe the Veselago lens effect predicted for massless Dirac fermions in a graphene nanoribbon with an ideally sharp p–n junction ($d \rightarrow 0$, see figure 3(a)). The source point \mathbf{x}_S of the incoming electric current is located at the center of the ribbon at a distance $|\mathbf{x}_S|$ from the interface larger than the

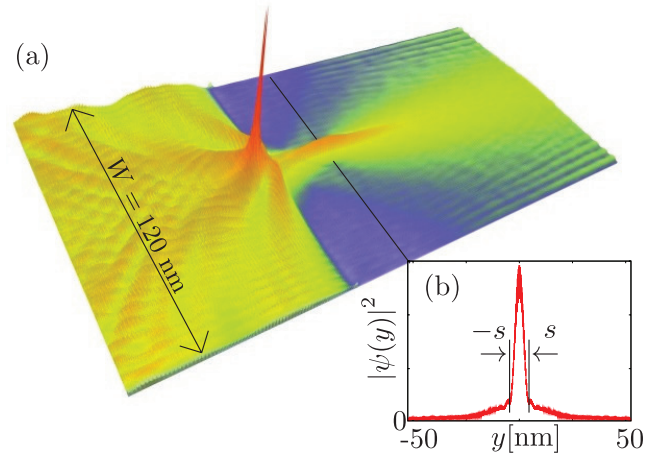


Figure 3. (a) Propagated wave $|\psi_{\mathbf{x}_S}(\mathbf{x})|^2$ of a perfect p–n junction in graphene ($d = 0$, $W = 120$ nm) a potential step of $V_0 = 1$ eV in the absence of disorder. (b) Cut through (a) along the black line. The transverse width of the focused beam is $2s \approx \lambda_D$.

de Broglie wavelength λ_D . For a doping of $E = V_0 = 0.5$ eV corresponding to a p–n step height of $2V_0 = 1$ eV, λ_D follows from the relation

$$\lambda_D E = \hbar v_F \approx 3.5 \cdot \text{nm eV}, \quad (6)$$

as $\lambda_D \approx 7$ nm. Choosing the distance of S from the interface $|\mathbf{x}_S| = 25$ nm, we have $|\mathbf{x}_S|/\lambda_D \geq 3.5$ for which pronounced focusing effects are already expected. In order to prevent the reduction of the visibility of focusing by boundary reflections, W should be large compared to $|\mathbf{x}_S|$, $W \gg |\mathbf{x}_S|$. Combining these two constraints implies $W \gg \lambda_D$ indicating that only in wide p–n junctions Veselago lens and Klein collimation are clearly visible. We observe focusing of the ray down to the diffraction limit with the lateral width s of the focal spot at F close to $2s \approx \lambda_D$. We have, furthermore, numerically verified that distributing the source point over a small area S of size λ_D^2 does not significantly change the focusing pattern. Likewise, a finite energy resolution ΔE , as long as $\Delta E \ll E$, does not substantially affect the quality of the focusing. However, even in this ideal limit of a sudden potential step (i.e. $d = 0$ in

equation (2)) small deviations from the Dirac picture such as trigonal warping [8, 37] become visible. Consequently, when changing from the electron to the hole cone, the conservation of k_y is not perfect, leading to a slight asymmetry in the distance of focal point F and source S from the p–n junction.

4. Measures for focusing and collimation

In order to quantitatively characterize in the following focusing and collimation properties in realistic p–n graphene junctions we introduce as a measure for finding the electron inside the spot width $(-s, s)$ of an ideal Veselago lens with $2s = \lambda_D$ (see figure 3(b)) the probability

$$P(x; s) = \frac{1}{A(x)} \int_{-s}^s |\psi(x, y)|^2 dy, \quad (7)$$

where the normalization constant $A(x)$ is determined by $P(x; s = W/2) = 1$. We furthermore introduce the contrast C ,

$$C(x) = \frac{1}{A'} (\max(|\psi(x)|^2) - \min(|\psi(x)|^2)) \quad (8)$$

characterizing the visibility of focusing regardless of its location within the p domain. Equation (7) remains applicable also in cases where the focal point is displaced relative to the position F predicted for the ideal Veselago lens. The normalization A' in equation (8) will be kept fixed at $C(x) = 1$ for the ideally sharp p–n junction to allow a direct comparison between the contrast for different realizations of p–n junctions.

5. Finite transition width

As a first step towards a realistic scenario for a p–n junction we consider a finite transition (half)width d of an otherwise ideal junction. We observe a gradual change from the Veselago-lens type focusing (for $2d = 0.5 \text{ nm} \ll \lambda_D$, figure 4(a)) to the low-divergence beam filter (for $2d = 15 \text{ nm} > \lambda_D$, figure 4(d)) predicted by Cheianov *et al* [28]. This beam shaping and collimation is not an immediate consequence of the negative index of refraction itself but of the filtering out of large-angle momentum components incident on the junction, i.e. filtering due to imperfect Klein tunneling at larger angles of incidence [18]. For the linear potential step (equation (2)), the filtering out of larger angles of incidence α ($\alpha = 0$ denotes perpendicular incidence) can be analytically estimated in terms of an effective tunnel probability of [28]

$$p(\alpha) = \exp[-2\pi^2 d / \lambda_D \sin^2 \alpha]. \quad (9)$$

The range of transmitted angles is thus controlled by the ratio d/λ_D . For small α , equation (9) will yield probabilities close to one even for large d (indeed, at $\alpha = 0$, any finite d will lead to perfect transmission). For larger angles of incidence, however, only p–n junctions with small transition widths will allow for transmission, leading to the beam-like pattern we observe in our numerical simulations. While the beam formed by such a Klein collimator is well focused with width $2s \approx \lambda_D$, its total amplitude is, of course, reduced with increasing transition width d in the regime $d \gg \lambda_D$, leading to a reduction of

the absolute contrast (see figure 4(e)). Spatially extended p–n junctions thus allow for the formation of a tightly focused electron beam with interesting applications such as collision-free ballistic transport of the confined beam due to the suppression of interactions with (rough) edges of nanoribbons.

The potential height V_0 provides a second tuning parameter for the p–n junction. For optimal Klein tunneling the Fermi level E_F is tuned by doping to coincide with V_0 (figure 1). For smaller V_0 , the increased electron wavelength decreases the resolution of the interference structures (compare figures 5(a)–(d)). Moreover, for very small V_0 and correspondingly large λ_D the focal spot width increases resulting in a decrease of P and C (figure 5(e)). On the other hand for V_0 too large ($\geq 0.7 \text{ eV}$), effects of the nonlinear band bending far away from the Dirac point decrease the focusing efficiency and the contrast (figure 5(e)). Simultaneously decreasing the transition width d , V_0 and E_F , while keeping the ratio λ_D/d constant, improves transmission in disorder-free junctions [16]: at small energies, and thus large λ_D , a soft junction (featuring a transition length of the order of λ_D , yet large compared to the lattice constant) transmits better than a sharp one. However, experimental realizations require robustness of focusing against finite long-range disorder (as induced, e.g. by the substrate) providing a lower bound for V_0 .

6. Disorder and interface roughness

Creating a potential step with a strong gradient in the electronic potential that varies by a fraction of an eV over a few nanometers for a p–n junction in a realistic device still poses a considerable challenge. This requires fabrication techniques beyond simple back-gate voltages, e.g. etching of contacts very close to the graphene membrane, or top-gate approaches [14]. Such approaches, however, invariably introduce some level of roughness, i.e. deviation from a straight interface perpendicular to the ribbon axis (see figure 2). Simulation of a realistic scenario for the realization of such nanoscale electron-optical structures requires the inclusion of corrugation of the p–n interface. Such interface roughness Δx limits focusing and contrast unless it is negligibly small compared to the de Broglie wavelength λ_D . The focusing parameter P and the contrast C remain high for $\Delta x \lesssim \lambda_D$ but rapidly decrease for larger Δx (figure 6(a)). Clearly, the effect of interface roughness could be reduced by increasing λ_D . The latter can be achieved by reducing the energy separation V_0 between the n- and p- regions. However, as the size of the focal spot also scales with λ_D , suppression of interface roughness would come at the expense of a reduced contrast.

A second limitation for a realistic graphene nanoribbon is bulk disorder, in particular due to interaction with the substrate. Disorder limits electron mobility and can cause a transport gap in quantum dot measurements [4]. To investigate the influence of such a disorder on electron-optical properties, we include a bulk disorder potential in the n- and p-regions (see figure 2(d)). We use a correlated disorder potential $V_D(\mathbf{x})$, with an amplitude $\langle V_D \rangle$ and an autocorrelation length ξ in both the n- and p-regions. A well-defined junction requires of course that local potential variations are smaller than the

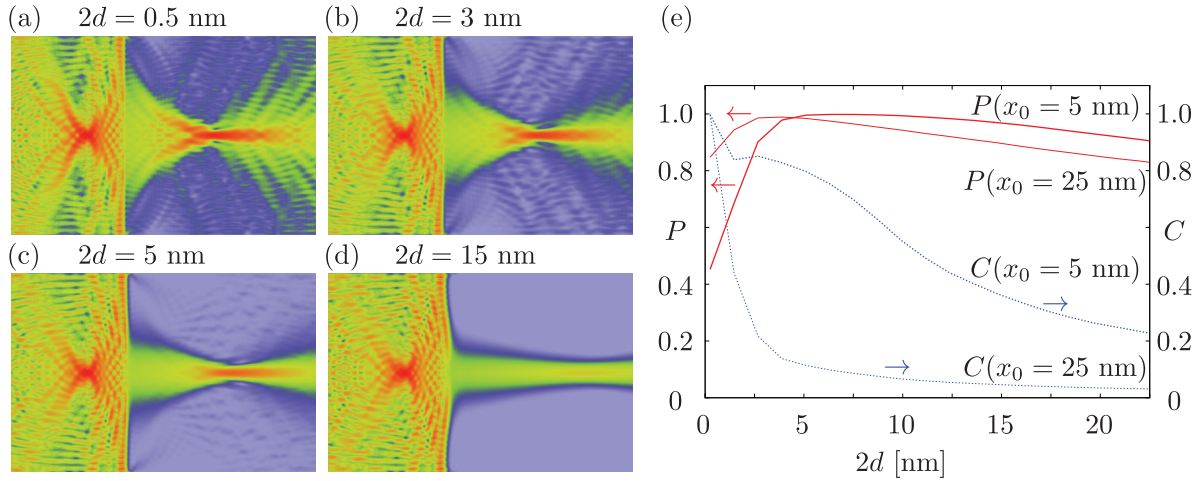


Figure 4. (a)–(d) Propagated wave $|\psi_{\mathbf{x}_S}(\mathbf{x})|^2$ near a p–n junction with width $W = 120 \text{ nm}$ featuring different transition region widths $2d$ (see insets, equation (2)) and a step height of $V_0 = 500 \text{ meV}$. The source point \mathbf{x}_S is 25 nm away from the onset of the p–n junction. (e) Contrast C (equation (8)) and focusing probability P (equation (7)) of an ideal p–n junction as a function of transition width for different distances $|x_S|$ from the junction (see insets). (a) $2d = 0.5 \text{ nm}$. (b) $2d = 3 \text{ nm}$ (c) $2d = 5 \text{ nm}$ (d) $2d = 15 \text{ nm}$.

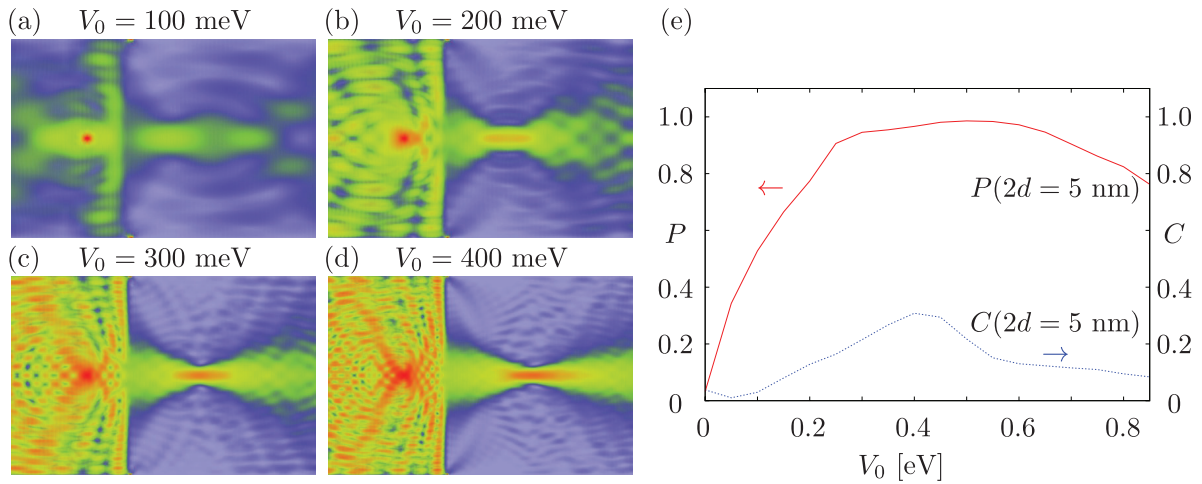


Figure 5. (a)–(d) Propagated wave $|\psi_{\mathbf{x}_S}(\mathbf{x})|^2$ of a p–n junction of width $W = 120 \text{ nm}$ for different potential step heights V_0 (see insets, equation (2)) at fixed transition width of $2d = 5 \text{ nm}$. Source point at a distance of 25 nm away from the p–n junction. (e) Contrast C (equation (8)) and focusing probability P (equation (7)) of the p–n junction as a function of step height V_0 . (a) $V_0 = 100 \text{ meV}$. (b) $V_0 = 200 \text{ meV}$ (c) $V_0 = 300 \text{ meV}$ (d) $V_0 = 400 \text{ meV}$.

potential step of the junction, $V_D \ll V_0$. As expected, the effect of disorder is strongest when the correlation length ξ matches the de Broglie wavelength, $\xi \approx \lambda_D$, while it is reduced for both longer and shorter correlation lengths. The latter applies only as long as the correlation length is still large compared to the lattice spacing, $a \ll \xi \leq \lambda_D$. For very short correlation lengths of the order of the lattice spacing characteristic for lattice point defects, strong inter-valley scattering, a peculiarity of graphene, can severely impede well-defined electron-optical properties. It should be noted that Klein tunneling itself is not directly affected by bulk disorder but the lensing effect is. As a result, we observe several local maxima rather than a single focal point (see figure 6(b)). Accordingly, the probability P of finding the electron in the focal region is significantly reduced with increasing potential strength $\langle V_D \rangle$, while the contrast C decreases only slowly (see figure 6(b)). Up to a disorder potential of the order of $\langle V_D \rangle \approx 0.1 \text{ eV}$ corresponding to

$$\langle V_D \rangle / V_0 \approx 0.2, \quad (10)$$

the contrast is still above the 50% level. At the same time, the height of the potential step should be smaller than the characteristic energies associated with the interface corrugation,

$$E_{\Delta x} = \hbar v_F k_{\Delta x} \quad \text{and} \quad E_d = \hbar v_F k_d \quad (11)$$

with $k_{\Delta x} = 2\pi/\Delta x$ and $k_d = 2\pi/d$. Combining the constraints (10) and (11) provides a criterion for the admissible potential height V_0 ,

$$5\langle V_D \rangle \lesssim V_0 \lesssim 2\pi\hbar v_F \frac{1}{d + \Delta x} \quad (12)$$

for which focusing and collimation should be observable. We emphasize that these bounds apply to fully phase-coherent single-electron transport.

In the present simulation we do not explicitly treat sublattice-breaking disorder $V_\sigma \propto \sigma_z$, where the Pauli matrix σ_z acts

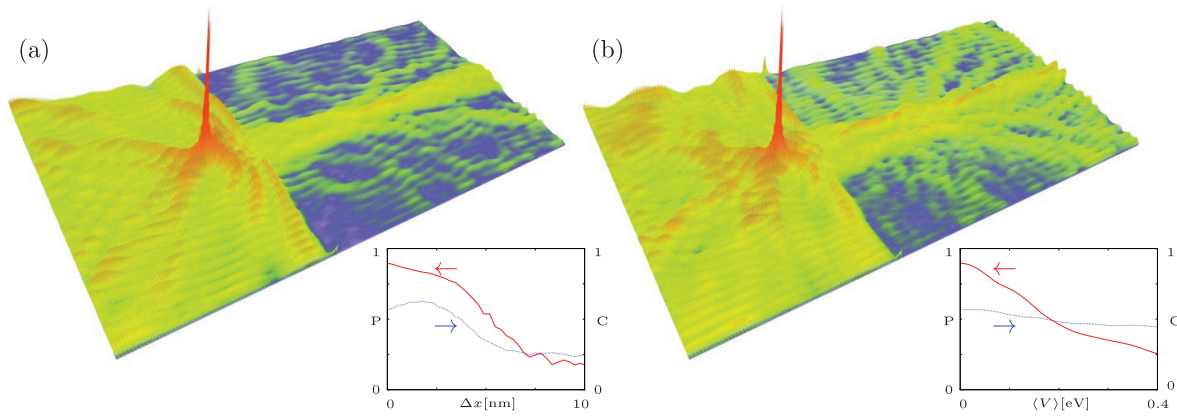


Figure 6. (a) Propagated wave $|\psi_{\mathbf{x},s}(\mathbf{x})|^2$ near a p–n junction of step height $V_0 = 500$ meV, width $W = 120$ nm with a rough interface $\Delta x = 5$ nm. The inset shows the evolution of focusing probability P (solid line, see equation (7)) and the contrast C (dashed line, see equation (8)) as a function of interface roughness Δx . (b) Same as (a) for a p–n junction with bulk disorder potential $V_D(\mathbf{x})$, $\langle V \rangle = 0.2$ eV. The inset shows P and C as a function of mean disorder potential amplitude $\langle V \rangle$.

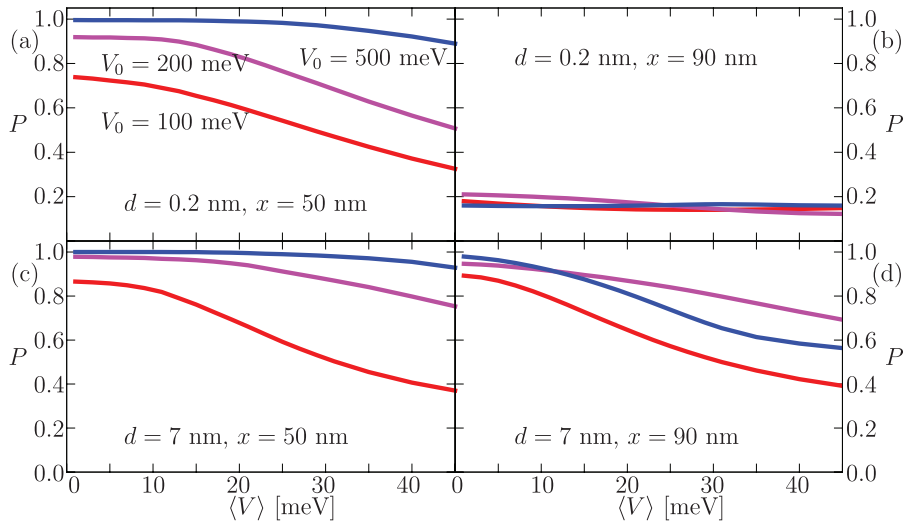


Figure 7. Focusing probability P (equation (7)) as a function of averaged disorder strength $\langle V \rangle$ for three different step heights V_0 of the p–n junction (see insets), evaluated for a junction with narrow transition region ($d = 0.2$ nm, top row) and a wide transition region ($d = 7$ nm, bottom row). P is evaluated at distance $x = 50$ nm (left column) and $x = 90$ nm (right column) from the p–n junction. Width W of the ribbon is 300 nm, calculation based on the Dirac approximation of equation (1).

on the sublattice degree of freedom. The potential V_σ implies different local potentials on the two trigonal sublattices of graphene. Such short-range fluctuations are induced, e.g. by substrates such as hexagonal boron nitride. Depending on the relative alignment of the graphene layer with respect to the substrate, the two sublattices of graphene positioned, e.g. over a boron and a nitrogen atom may see quite different potentials [38]. The resulting V_σ opens a band gap at the Dirac point. We have verified numerically that potentials of the order of 10% of the step height V_0 do not strongly affect the focusing properties of the p–n junction.

Testing our predictions (equation (12)) for smaller disorder strength $\langle V \rangle$ and step heights V_0 (and thus larger wave lengths) requires larger system sizes. We simulate a junction of width $W = 300$ nm (i.e. about a factor three wider than the p–n junctions discussed above). For these simulations, we solve the Dirac equation (1) in the continuum limit rather

than the TB Schrödinger equation for numerical simplicity thereby neglecting effects due to the discrete lattice structure. As expected, the small asymmetry of the transmitted wave due to trigonal warping disappears entirely. Consequently, these results can give only an upper bound for the quality of focusing for realistic graphene. We find the same qualitative trends as before: the focusing probability P decreases with increasing disorder strength (figure 7). Klein collimation for larger d is more robust to disorder (compare bottom and top row of figure 7). Efficient focusing at larger disorder amplitudes requires larger step heights. While larger disorder even increases the overall transmission of the p–n junction, in line with previous results [31], the focusing decreases rapidly (see figure 8).

A comparison to recent experiment further corroborates our analysis. Lee *et al.* realized a transition width of $d \approx 12$ nm using a top gate made of few-layer hexagonal boron nitride [27]. They consider a series of two junctions (i.e. a

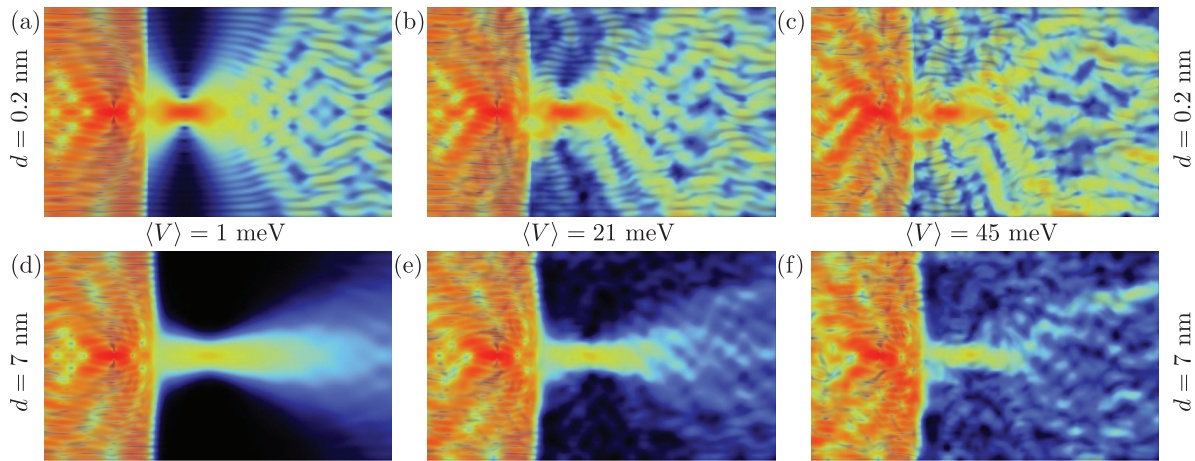


Figure 8. Propagated wave $|\psi_{x_s}(\mathbf{x})|^2$ near a p-n junction of width $W = 300$ nm for different disorder strength $\langle V_0 \rangle = 1$ meV, 21 meV and 45 meV (left to right) and transition halfwidth $d = 0.2$ nm (top) and $d = 7$ nm (bottom).

p-n-p and n-p-n transition), and find a small but discernable enhancement of transmission of the order of 5% due to the Veselago lens effect. Estimating the step height in this experimental device with a gate coupling $\eta \approx 7.2 \times 10^{10} \text{ cm}^{-2} \text{ V}^{-1}$ yields for a gate voltage V_G of 10V a doping level of $n = \eta V_G \approx 2.3 \times 10^{12} \text{ cm}^{-2}$, or a Fermi level of [27]

$$E_F = \hbar v_F \sqrt{\pi n} \approx 100 \text{ meV}, \quad (13)$$

i.e. the value used in our calculations for figure 8. The experiment estimates disorder by a mean free path Λ_{mfp} of $\Lambda_{\text{mfp}} \approx 1.7 \mu\text{m}$. To compare to the disorder scale of our calculations we determine numerically a mean free path associated with our randomly correlated disorder. We find $\Lambda_{\text{mfp}} \approx 1.7 \mu\text{m}$ for a disorder strength of $\langle V \rangle = 20$ meV using a fit to averaged transmission coefficients [39, 40]. Our calculations yield a P value of 0.45 for this disorder strength (see lowest curve in figures 7(a and c)), suggesting an upper bound for the focusing probability of two junctions of 20% in fair agreement with the experimental findings of a 5% enhancement [27]. Testing our relation for the energy scales equation (12)

$$5\langle V_D \rangle \approx 100 \text{ meV} \lesssim V_0 \approx 100 \text{ meV} \lesssim 2\pi\hbar v_F \frac{1}{\Delta x + d} \approx 250 \text{ meV}, \quad (14)$$

confirms that the experiment is within our suggested bounds for observing the Veselago lens effect. Indeed, the tight constraint $V_D \leq \langle V_0/5 \rangle$ might explain the comparatively small enhancement of the transmitted current found in the experiment. We thus conclude that the quantitative bounds we provide are a good indicator for the suitability of an experimental setup to exploit electron focusing by p-n junctions.

7. Conclusions

We have investigated electron-optical focusing and filtering in realistic graphene devices generalizing the notion of a Veselago lens based on Klein tunneling of massless Dirac fermions. We find that the focusing effect is robust against moderate disorder and give quantitative upper bounds for the distortion by bulk disorder and interface roughness. The major

challenge in experimental realization remains achieving sharp potential steps necessary for Klein tunneling. Comparing junctions of different step height, we find that lower step heights show better focusing for zero bulk disorder, yet suffer more strongly from finite disorder. Comparing our prediction with recent experiment indicates an optimized setting when the junction height is about an order of magnitude larger than the average bulk disorder.

Acknowledgments

We thank V Cheianov, M Katsnelson, M Morgenstern, and C Stampfer for valuable discussions. Support from the ViCoM SFB-041 are gratefully acknowledged. L A gratefully acknowledges support by FWF project 23359-N16. Numerical calculations have been performed on the Vienna Scientific Cluster (VSC2 and VSC3).

References

- [1] Han M Y, Özyilmaz B, Zhang Y and Kim P 2007 *Phys. Rev. Lett.* **98** 206805
- [2] Chen Z, Lin Y, Rooks M and Avouris P 2007 *Physica E* **40** 228
- [3] Ponomarenko L A, Schedin F, Katsnelson M I, Yang R, Hill E H, Novoselov K S and Geim A K 2008 *Science* **320** 356
- [4] Stampfer C, Güttinger J, Hellmüller S, Molitor F, Ensslin K and Ihn T 2009 *Phys. Rev. Lett.* **102** 056403
- [5] Geim A K and Novoselov K S 2007 *Nat. Mater.* **6** 183
- [6] Trauzettel B, Bulaev D V, Loss D and Burkard G 2007 *Nat. Phys.* **3** 192
- [7] Freitag N *et al* 2016 *Nano Lett.* **16** 5798
- [8] Neto A H C, Guinea F, Peres N M R, Novoselov K S and Geim A K 2009 *Rev. Mod. Phys.* **81** 109
- [9] Katsnelson M I 2012 *Graphene: Carbon in Two Dimensions* (Cambridge: Cambridge University Press)
- [10] Novoselov K S, Geim A K, Morozov S V, Jiang D, Katsnelson M I, Grigorieva I V, Dubonos S V and Firsov A A 2005 *Nature* **438** 197
- [11] Zhang Y, Tan Y-W, Stormer H and Kim P 2005 *Nature* **438** 201

- [12] Berry M V and Mondragon R J 1987 *Proc. R. Soc. Lond. A* **412** 53
- [13] Terrés B et al 2016 *Nat. Commun.* **7** 11528
- [14] Young A F and Kim P 2009 *Nat. Phys.* **5** 222
- [15] Klein O 1929 *Z. Phys. A: Hadr. Nucl.* **53** 157
- [16] Logemann R, Reijnders K J A, Tudorovskiy T, Katsnelson M I and Yuan S 2015 *Phys. Rev. B* **91** 045420
- [17] Tudorovskiy T, Reijnders K J A and Katsnelson M I 2012 *Phys. Scr. T* **146** 014010
- [18] Reijnders K J A, Tudorovskiy T and Katsnelson M I 2013 *Ann. Phys.* **333** 155
- [19] Veselago V G 1968 *Sov. Phys.—Usp.* **10** 509
- [20] Cheianov V V, Fal’ko V I and Altshuler B L 2007 *Science* **315** 1252
- [21] Shalaev V M 2007 *Nat. Photon.* **1** 41
- [22] Pile D 2015 *Nat. Photon.* **9** 210
- [23] Landy N and Smith D R 2013 *Nat. Mater.* **12** 25
- [24] Brunet T, Merlin A, Mascaro B, Zimny K, Leng J, Poncelet O, Aristégui C and Mondain-Monval O 2015 *Nat. Mater.* **14** 384
- [25] Dean C R et al 2010 *Nat. Nanotechnol.* **5** 722
- [26] Wang M et al 2013 *Adv. Mater.* **25** 2746
- [27] Lee G-H, Park G-H and Lee H-J 2015 *Nat. Phys.* **11** 925–9
- [28] Cheianov V and Fal’ko V I 2006 *Phys. Rev. B* **74** 041403
- [29] Fogler M M, Novikov D S, Glazman L I and Shklovskii B I 2008 *Phys. Rev. B* **77** 075420
- [30] Rossi E, Bardarson J H, Brouwer P W and Das Sarma S 2010 *Phys. Rev. B* **81** 121408
- [31] Long W, Sun Q-F and Wang J 2008 *Phys. Rev. Lett.* **101** 166806
- [32] Katsnelson M I, Novoselov K S and Geim A K 2006 *Nat. Phys.* **2** 620
- [33] Wallace P R 1947 *Phys. Rev.* **71** 622
- [34] Libisch F, Stampfer C and Burgdörfer J 2009 *Phys. Rev. B* **79** 115423
- [35] Amestoy P R, Duff I S, Koster J and L’Excellent J-Y 2001 *SIAM J. Matrix Anal. Appl.* **23** 15
- [36] Amestoy P R, Guermouche A, L’Excellent J-Y and Pralet S 2006 *Parallel Comput.* **32** 136
- [37] McCann E, Kechedzhi K, Fal’ko V I, Suzuura H, Ando T and Altshuler B L 2006 *Phys. Rev. Lett.* **97** 146805
- [38] Chizhova L A, Libisch F and Burgdörfer J 2014 *Phys. Rev. B* **90** 165404
- [39] Doppler J, Méndez-Bermúdez J A, Feist J, Dietz O, Krimer D O, Makarov N M, Izrailev F M and Rotter S 2013 *New J. Phys.* **16** 053026
- [40] Chizhova L A, Libisch F and Burgdörfer J 2016 *Phys. Rev. B* **94** 075412